

Topological pumping in atomtronic circuits

Tobias Haug,¹ Rainer Dumke,^{1,2,3} Leong-Chuan Kwek,^{1,3,4,5} and Luigi Amico^{1,3,6,7,8}

¹Centre for Quantum Technologies, National University of Singapore, 3 Science Drive 2, Singapore 117543, Singapore

²Division of Physics and Applied Physics, Nanyang Technological University, 21 Nanyang Link, Singapore 637371, Singapore

³MajuLab, CNRS-UNS-NUS-NTU International Joint Research Unit, UMI 3654, Singapore

⁴Institute of Advanced Studies, Nanyang Technological University, 60 Nanyang View, Singapore 639673, Singapore

⁵National Institute of Education, Nanyang Technological University, 1 Nanyang Walk, Singapore 637616, Singapore

⁶Dipartimento di Fisica e Astronomia, Via S. Sofia 64, 95127 Catania, Italy

⁷CNR-MATIS-IMM & INFN-Sezione di Catania, Via S. Sofia 64, 95127 Catania, Italy

⁸LANEF 'Chaire d'excellence', Université Grenoble-Alpes & CNRS, F-38000 Grenoble, France

(Dated: September 6, 2022)

The progress in cold atom quantum technology enable the creation of matter wave circuits confined in optically and magnetically generated guides with unprecedented flexibility and control. Recent achievements in this field allow to manipulate circuits in time and on micrometer scales. To highlight on these technological breakthroughs, we engineer local driving in atomtronic circuits to realize topological pumping. Specifically, we study the interplay of topological pumping with the topological phase winding created by an Aharonov-Bohm flux in a bosonic ring condensate. We demonstrate that the Aharonov-Bohm effect in our system emerges from transitions between the topological bands. We find that flux quantization, transmission and type of pumped states become highly dependent on interaction, number of particles, the topological band and size of the ring. The pumping can create entangled states in the ring which yield non-trivial interference pattern.

Introduction. Topological matter defines an important field in fundamental physics with far reaching implications for quantum technology: the correlations encoded in topological matter are a precious resource for quantum technology; at the same time, quantum technology can be exploited to study topological matter with unprecedented precision and control[1–4]. Among the several important contributions given by David Thouless in this field, the idea of topological pumping is particularly relevant for quantum technology: charge is transported through a one dimensional system using the topological band structure of an extended (many-body) system[5, 6]. This is realized by driving the system periodically in time while protecting the band gaps. Topological pumping has been studied with the most recent approaches in experimental quantum technology, from cold atoms[7–9], photonic waveguides[10] and superconducting circuits[11].

Here, we couple topological bands with Atomtronics: atomic circuits of ultra-cold atoms manipulated in micro-magnetic or laser-generated micro-optical guides [12–14]. Clearly, this design implies several advantages compared to electron-based networks, including a reduced decoherence rate due to charge neutrality of atomic currents, the ability to play with fermionic or bosonic carriers and change intrinsic parameters like the carrier-carrier interaction. By investigating quantum transport with such new twists [15–18], the scope of cold atoms quantum technology can be enlarged for quantum simulation, quantum devices and quantum sensors[19].

There has been much interest in elementary atomtronic circuits made of a bosonic condensate flowing in a ring-shaped guide and pierced by an effective magnetic field [20–31]. Recent progress in the integration of the know-how in cold atom quantum technology and micro-optics allows to construct more complex circuits with new functionalities: condensates can be loaded in basically arbitrary potentials with micron-scale resolution [32, 33]. In particular, Digital Mi-

romirror Devices (DMD) can update the shape and intensity of optical potentials in time scales of tens to hundreds microseconds. These remarkable advances allow to modulate the local features of the circuit in time during experiments [34–37].

In this paper we study the local driving of atomtronic circuits to highlight these new perspectives in cold atoms quantum technology. In particular, we analyze the interplay between topological pumping and Aharonov-Bohm (AB) phase winding in interacting bosonic systems for which several new features have been evidenced recently[38, 39] (for topological pumping in non-interacting rings see [40, 41]). We note that since topological pumping is robust to disorder and particle loss [11, 42], by our approach we can further enhance the flexibility of Atomtronics.

Summary of the results. The setup is depicted in Fig.1 – see Eqs.1, 2, 3. The system is characterized by topologically distinct bands that can be addressed feasibly by changing the parameter of the driving (its phase ϕ_0)—see Fig.2a,b. Interaction, AB oscillations and the topology of the bands couple together in a non-trivial way. As a result, a complex variety of flux quanta, types of entangled states and transmission coefficients are found. In particular, we understand that AB oscillations in our circuit result from transitions between the topological bands. Interestingly enough, the source-ring and the ring-drain interfaces act as non-linear matter-wave interferometers: NOON states between lower and upper arms of the ring can be generated—see Fig.2c. The speed of the state preparation and the robustness to disorder is limited by Landau-Zener transitions between bands; the curvature of the band implies different methods of transitions (resonant and off-resonant) —see Fig.2b. The lowest band is the best band for the transport of N atoms as the band gap scales $\propto \sqrt{N}$.

The states are transported through the ring, and interfere in the drain. The transmission depends on the applied AB

flux and different (entangled) states make it periodic with a characteristic flux quantum Φ_0 depending on the particle number (see Figs.3, 4b): for the lowest topological band and even number of particles the density of the pumped particles does not depend on the AB flux; for odd number of particles, instead, the density of the pumped particles results in a non-trivial interference pattern –see Fig.4a. The central band of the system can generate different types of partial transmission, parity effects and (entangled) states depending on the initial phase shift of the potential and the length of the ring –see Fig.5. By analyzing the dynamics of the system, we evidence that the curvature of the band leads to a partial particle pumping with AB flux. Our results are schematically summarized in Table I.

Model and methods. A sketch of the ring-lead system is presented in Fig.1a. It is composed of a lattice ring attached

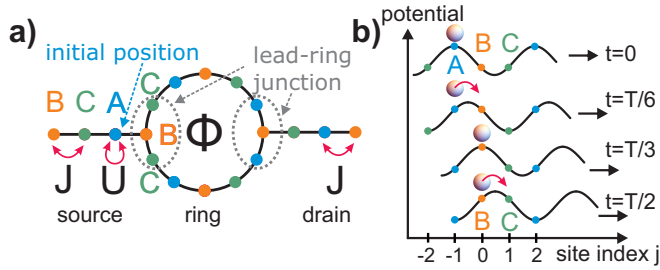


FIG. 1. **a)** Sketch of the ring-lead system. The dots indicate lattice sites j with local potential $V_j(t) = \cos(2\pi/3j - \Omega t)$ with a period of three lattice sites (A: $j = 0$, B: $j = 1$, C: $j = 2$). Particles tunnel between different sites along the black lines with strength J . U denotes the on-site interaction and Φ the flux of the ring. **b)** Topological pumping of particles on lattice sites by adiabatic modulation of the periodic potential $V_j(t)$ with Chern number $C = -1$. The cosine potential (black line) is varied adiabatically in time t with a frequency $\Omega = 2\pi/T$, where T is the time of one driving period. Particles are initialized at A. At time $t = 0$ no tunneling occurs due to a large potential difference to neighboring sites. At time $t = 1/6T$, potential of A and B is degenerate, and particles are adiabatically transferred to B. After one period T the particles have moved by 3 sites.

to two leads (source and drain) symmetrically at two opposite sites of the ring loaded with N particles. The ring-lead Hamiltonian is $\mathcal{H} = \mathcal{H}_R + \mathcal{H}_S + \mathcal{H}_D + \mathcal{H}_I + \mathcal{H}_P$. The ring Hamiltonian is

$$\mathcal{H}_R = - \sum_{j=1}^{L_R} (J e^{i2\pi\Phi/L} \hat{a}_j^\dagger \hat{a}_{j+1} + \text{H.C.}) + \frac{U}{2} \sum_{j=1}^{L_R} \hat{n}_j^a (\hat{n}_j^a - 1), \quad (1)$$

where \hat{a}_j and \hat{a}_j^\dagger are the annihilation and creation operator at site j in the ring, L_R the number of ring sites, $\hat{n}_j^a = \hat{a}_j^\dagger \hat{a}_j$ is the particle number operator of the ring, J is the inter-site hopping, U is the on-site interaction between particles and Φ is the total flux through the ring. Periodic boundary conditions are applied for the ring with $\hat{a}_{L_R}^\dagger = \hat{a}_0^\dagger$. In the following, we set $J = 1$, and all values of U , Ω are given in units of J . The lead

Hamiltonian for source (similar for drain \mathcal{H}_D) is given by

$$\mathcal{H}_S = - \sum_{j=1}^{L_S} (J \hat{s}_j^\dagger \hat{s}_{j+1} + \text{H.C.}) + \frac{U}{2} \sum_{j=1}^{L_S} \hat{n}_j^s (\hat{n}_j^s - 1), \quad (2)$$

where L_S (L_D) is the length of the source (drain) and \hat{s}_j (\hat{d}_j) the source (drain) annihilation operator. We set $L_S = L_D = 1$ in the following. The coupling Hamiltonian between leads and ring is $\mathcal{H}_I = -J (\hat{a}_0^\dagger \hat{s}_0 + \hat{a}_{L_R/2}^\dagger \hat{d}_0 + \text{H.C.})$. We modulate the potential landscape adiabatically to pump particles

$$\mathcal{H}_P(t) = P_0 \sum_j \cos\left(\frac{2\pi j}{3} - \phi_0 - \Omega t\right) \hat{n}_j, \quad (3)$$

with the driving frequency Ω , the particle number operator \hat{n}_j at site j of the system and phase shift ϕ_0 . The potential has a period of three sites and its arrangement in the ring-lead system is shown in Fig.1a. In the case of zero interaction and no flux, the Hamiltonian is known to be topological nontrivial with three bands and non-zero Chern numbers [6] (top +1 and bottom -1 band has Chern number $C = -1$ and central band 0^\pm has $C = 2$). The pumping is induced by breaking time-translational symmetry via driving. The topological properties hold true within perturbation theory even in the interacting case [11]. Similar systems have been studied in [11, 43]. After one period of the time evolution $T = 2\pi/\Omega$, particles move by $3C$ sites (see Fig.1b). The protocol is as follows: Initially, a Fock state with N particles is prepared at a single site in the source lead. Here, we initialize the particle at the first source lead site that directly neighbors the ring and use ϕ_0 to select the band (see Fig.1a).

The equations of motions are solved with exact diagonalization, by evolving the Schrödinger equation $|\Psi(t)\rangle = e^{i\mathcal{H}t} |\Psi(0)\rangle$.

In the following, we investigate positive interaction $U > 0$ without losing generality. For $U < 0$, simply switch the results of band +1 with -1, and 0^+ with 0^- . We operate in the limit of $P_0 \gg J, U$, such that the eigenstates are strongly localized within single sites. Thus, tunneling between neighboring sites is suppressed (since they have in general a widely different local potential), as well as effective tunneling across three sites (to the nearest site with the same potential). To fulfill the adiabatic criterion $\Omega \ll J, U, P_0$. We characterize the dynamics in terms of transmitted density into the source after a single pumping iteration (when particles reach the drain for the first time).

Topological pumping. For a single particle or $U = 0$ the flux dependence and smallest energy gap $\Delta E = 2J$ is the same for all bands. The speed of pumped particles solely depends on the Chern number of its band. We see the standard AB effect with full transmission through the ring for zero flux, and total reflection due to destructive interference at half-flux. Remarkably, reflections occur by transitions into bands with Chern number of opposite sign, such that the particle moves into the reverse direction. However, we believe they are distinct from Landau-Zener transitions as they occur for even very slow driving frequency.

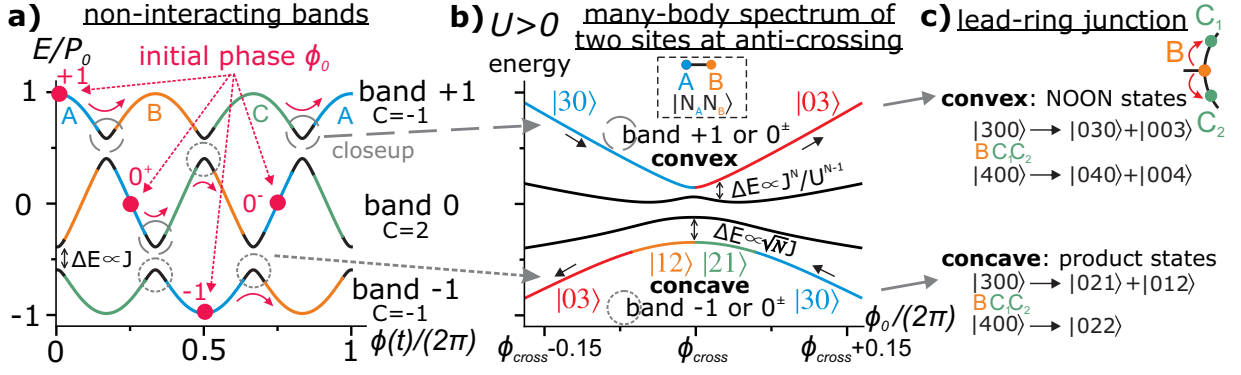


FIG. 2. **a)** Non-interacting topological pumping with three bands. Particles are initialized at site A (blue region), corresponding to different initial phase shifts ϕ_0 for each band. For band 0 (Chern number $C = 2$), two different initial ϕ_0 are possible, with different dynamics. Particles initialized in a band follow it adiabatically by varying $\phi(t)$ and are pumped between the sites A-B-C. The energy gap for the non-interacting model is $\Delta E \propto J$ for all bands. **b)** Close-up of the interacting eigenlevel structure of a band anti-crossing at the transition from one site to the next (indicated by the dashed circles) for positive interaction $U > 0$. During pumping, either top curve with positive curvature (convex, at crossings indicated by long dashed circles in a) in band +1 or 0) or bottom curve with negative curvature (concave, indicated by short dashed circles in band -1 or 0) is adiabatically followed. For convex, the energy gap to the next eigenstate is scaling as $\Delta E \propto J^N/U^{N-1}$ for $U \gg J$. The transport occurs due to off-resonant coupling of the final states ($|30\rangle$ and $|03\rangle$ for $N = 3$) with off-resonant intermediate states ($|21\rangle, |12\rangle$) which are not significantly occupied. For concave, the energy gap is $\Delta E = 2\sqrt{N}J$ for $U \gg J$. Transport occurs via resonant transitions to the intermediate states ($|21\rangle, |12\rangle$) which are significantly occupied. For $U < 0$, the behavior of the two bands are interchanged. **c)** At the lead-ring junction (see Fig. 1a), the two types of transitions will produce different end results: convex gives NOON states, while concave yields product states.

band $U > 0$	ring length L_R	Chern number	ϕ_0	AB period Φ_0	parity effect	transmission: N even		transmission: N odd		state in ring	band gap ΔE
						$\Phi = 0$	$\Phi = \Phi_0$	$\Phi = 0$	$\Phi = \Phi_0$		
+1	$2n$	-1	0	$1/N$	no	N	$N - 1$	N	$N - 1$	NOON	J^N/U^{N-1}
0^+	$4n + 2$	2	$\pi/2$	$1/N$	no	N	$N - 1$	N	$N - 1$	NOON	J^N/U^{N-1}
0^+	$4n$	2	$\pi/2$	$1/N$	yes	0	1	1	0	NOON	J^N/U^{N-1}
0^-	$4n$	2	$-\pi/2$	1	yes	0	0	1	0	product	J^N/U^{N-1}
0^-	$4n + 2$	2	$-\pi/2$	1	yes	N	N	N	$N - 1$	product	J^N/U^{N-1}
-1	$2n$	-1	π	1	yes	N	N	N	$N - 1$	product	$2\sqrt{N}J$
$U = 0$ all bands	$2n$			1	no	N	0	N	0	superposition	$2J$

TABLE I. Aharonov-Bohm (AB) period and number of particles transmitted after one topological pumping cycle through an AB ring with initially N particles. Results depend on pumped band, ring length, parity of particle number N and interaction (here $U > 0$). Bands are visualized in Fig. 2a. For $U < 0$, exchange the band indices \leftrightarrow (e.g. for $U < 0$ band +1 behaves like band -1 for $U > 0$).

We find that for increasing $|U| > \Omega$ the standard AB effect disappears, and instead we observe a many-body AB effect. Then, the pumping dynamics substantially depends on the band and the sign of U . The energy gap becomes dependent on band, interaction and particle number as well.

Lower band -1. Here, we choose $\phi_0 = \pi$ – see Fig. 2a. In this case, the local driving implies that the avoided crossing is approached from below (the concave band of Fig. 2b). The particle transfer from one site to the next is found to happen via resonant transitions to intermediate many-body states, whenever these states become resonant. For $U \gg J$, the energy gap is independent of U : $\Delta E = 2\sqrt{N}J$ (see supplementary materials). In this regime, we find that the pumping is parity dependent. The dynamics as particles are pumped through the ring for different particles numbers is plotted in Fig. 3. For $N = 2n$ all the particles reach the drain independently of the flux (Fig. 3e). For $N = 2n + 1$, instead, the magnetic flux drives a fractional transmission: For zero flux, all

particles are transported to the drain (Fig. 3a). However, for half-flux, one particle is reflected and the rest is transmitted (Fig. 3c). The back-reflection occurs at twice the speed in the central band with Chern number $C = 2$. The effect traces back to the different structure of the many-body states that are generated in the ring by the driving. We denote the wavefunction of a single particle in the upper half of the ring as $|\uparrow\rangle$, and $|\downarrow\rangle$ the wavefunction in the lower half of the ring. For $N = 2n$, the ring state is $|\Psi_{2n}\rangle = (|\uparrow\rangle \otimes |\downarrow\rangle)^n$ causing no interference. For $N = 2n + 1$, the state in the ring has the form $|\Psi_{2n+1}\rangle = (|\uparrow\rangle \otimes |\downarrow\rangle)^n \otimes (|\uparrow\rangle + |\downarrow\rangle)$; the last part of the wavefunction is the one causing interference. The resulting density pumped into the drain is shown in Fig. 4a. Incidentally, we note that the circuit with two atom species can provide entangled Bell states (see the supplementary material); fractional statistics as introduced in Ref. [44] could not generate a different type of entangled states, but it would change the flux quantum.

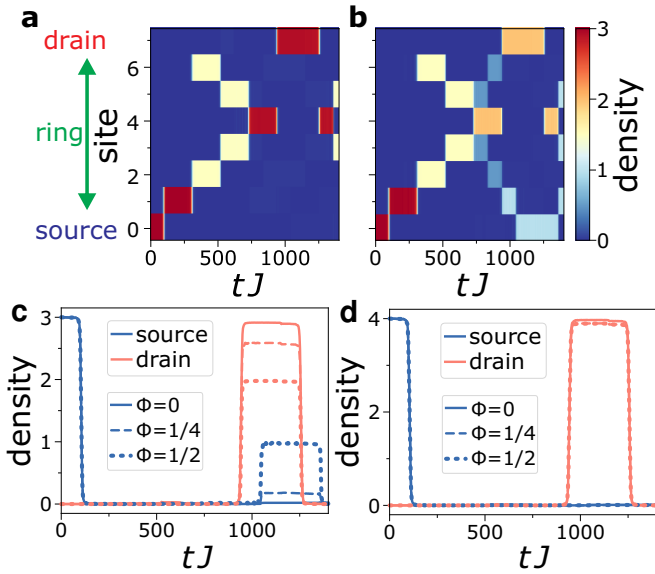


FIG. 3. Time evolution of topological pumping in the ring-lead system with $L_R = 6$, $U/J = 1$, $\Omega = 0.01J$, $P_0 = 40J$ in band -1. **a,b)** Density against time and sites for $N = 3$, **a)** flux $\Phi = 0$ and **b)** $\Phi = 1/2$. Site 0: source, site 1-6: ring, site 7: drain **c-d)** density in source and drain for particle numbers **c)** $N = 3$, **d)** $N = 4$.

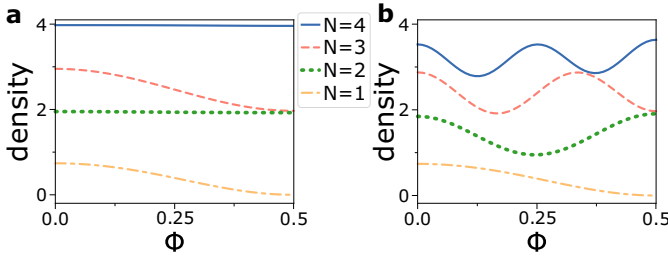


FIG. 4. Density pumped into the drain for **a)** band -1, $U = 0.5$ **b)** band +1 $U = 0.1$ Drain density measured at $tJ = 1260$ with $L_R = 8$, $\Omega = 0.01J$ and $P_0 = 60J$.

Upper band +1. Here, we choose $\phi_0 = 0$ so that the avoided crossing is approached from above – Fig.2b. The density in the drain after pumping is shown in Fig.4b. In this case, we find that tunneling between neighboring sites occurs via effective tunneling between off-resonant states via nearly resonant states that are weakly occupied during the transition (e.g. for $N = 3$ and $|N_j N_{j+1}\rangle$ denoting particles at neighboring sites j : when states $|30\rangle$ and $|03\rangle$ become resonant, they are off-resonantly coupled via the weakly occupied states $|21\rangle$ and $|12\rangle$). The effective coupling between the final states can be calculated with the Schrieffer-Wolff transformation [11]. Well defined AB oscillations are found: the AB minimum is at $\Phi = \frac{1}{2N}$. At the AB minimum, one particle is reflected, while the rest is transmitted for any number of particles or ring sites. The energy gap to the next band is $\Delta E \propto J^N / U^{N-1}$ ([45], see supplementary materials). The gap decreases sharply with increasing interaction U and the pumping is most efficient in the regime of small U . We observe NOON type superposition

between upper and lower part of the junction.

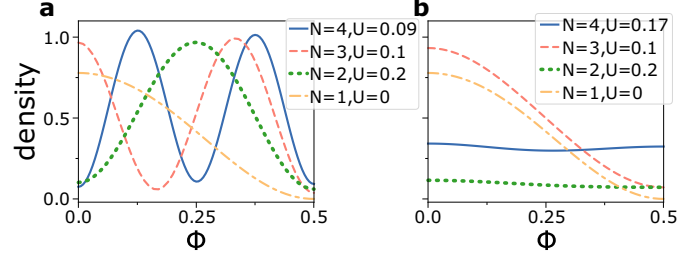


FIG. 5. Density pumped into the drain for central band 0 against flux for $U > 0$. **a)** band 0^+ ($\phi_0 = \pi/2$) **b)** 0^- ($\phi_0 = -\pi/2$). Drain density measured at $tJ = 630$, $\Omega = -0.01J$, $L_R = 8$ and $P_0 = 60J$.

Central band 0^\pm . The dynamics through the ring depends on the initial phase 0^+ ($\phi_0 = \pi/2$) or 0^- ($\phi_0 = -\pi/2$) (see Fig.2a). The transmission depends on the ring length L_R . For $L_R = 4n + 2$ and $U > 0$, the initial phase $\phi_0 = \pi/2$ has the same flux dependence as the upper band +1. For $\phi_0 = -\pi/2$ it behaves as the lower band; however, because of the different Chern number $C = 2$, the particles move at twice the speed and in opposite direction (thus exchange $\Omega \rightarrow -\Omega$). The anti-crossing curvature alternates between convex and concave (see Fig.2a) and the smallest energy gap scales as in band +1.

For $L_R = 4n$, the dynamics is quite different. For the band 0^+ (Fig.5a) the AB flux quantum is $\Phi_0 = 1/N$. The transmission is much lower and parity dependent: for even N , the transmission is zero for zero flux, and one particle for half a flux quantum. For odd N , we find the opposite behavior: one particle transmitted at zero flux, and zero transmitted at half flux-quantum. For band 0^- (Fig.5b), the flux quantum is $\Phi_0 = 1$. For even N , the transmission is zero, while for odd N it changes from one to zero with flux. The dependence on L_R comes from the switch between convex and concave transitions at every other site: For $L_R = 4n$, the transitions at source-ring and ring-drain approach the avoided crossing from opposite ways; this feature implies the change in transmission behavior. For $L_R = 4n + 2$, instead, the transmissions source-ring and ring-drain approach the avoided crossing from the same ways; this features implies that the transmission is similar to what found for the band ± 1 . In our numerical simulation, we see a finite probability of reaching the drain for even number of particles due to non-adiabatic transitions. The dependence on interaction is discussed in the supplementary materials.

Conclusions. We studied topological pumping in conjunction with an synthetic magnetic field in an interacting ring-lead system. We find that the interplay between topological bands and Aharonov-Bohm phase produces a complex variety of flux quanta, types of entangled states and transmission coefficients. Adiabatic shortcuts could allow to reduce the preparation time for the entangled states[46]. Relying on the established time-dependent light-shaping techniques available in quantum technology, we believe that our results are of immediate interest for the experiments. Our results are also rel-

evant for interacting photons in non-linear superconducting resonators. In these systems, topological pumping of interacting photons [11] and synthetic gauge fields [47] has been demonstrated.

Acknowledgments. We thank V. Bastidas, A. Daley and W. Munro for discussions. The Grenoble LANEF framework (ANR-10-LABX-51-01) is acknowledged for its support with mutualized infrastructure. We thank National Research Foundation Singapore and the Ministry of Education Singapore Academic Research Fund Tier 2 (Grant No. MOE2015-T2-1-101) for support. The computational work for this article was partially performed on resources of the National Supercomputing Centre, Singapore (<https://www.nsc.sg>).

-
- [1] J. M. Kosterlitz, *Rev. Mod. Phys.* **89**, 040501 (2017).
 [2] F. D. M. Haldane, *Rev. Mod. Phys.* **89**, 040502 (2017).
 [3] M. Z. Hasan and C. L. Kane, *Rev. Mod. Phys.* **82**, 3045 (2010).
 [4] J. P. Dowling and G. J. Milburn, *Philosophical Transactions of the Royal Society of London A: Mathematical, Physical and Engineering Sciences* **361**, 1655 (2003).
 [5] D. J. Thouless, M. Kohmoto, M. P. Nightingale, and M. den Nijs, *Phys. Rev. Lett.* **49**, 405 (1982).
 [6] D. Thouless, *Phys. Rev. B* **27**, 6083 (1983).
 [7] M. Lohse, C. Schweizer, O. Zilberberg, M. Aidelsburger, and I. Bloch, *Nat. Phys.* **12**, 350 (2016).
 [8] S. Nakajima, T. Tomita, S. Taie, T. Ichinose, H. Ozawa, L. Wang, M. Troyer, and Y. Takahashi, *Nat. Phys.* **12**, 296 (2016).
 [9] M. Lohse, C. Schweizer, H. M. Price, O. Zilberberg, and I. Bloch, *Nature* **553**, 55 (2018).
 [10] O. Zilberberg, S. Huang, J. Guglielmon, M. Wang, K. P. Chen, Y. E. Kraus, and M. C. Rechtsman, *Nature* **553**, 59 (2018).
 [11] J. Tangpanitanon, V. M. Bastidas, S. Al-Assam, P. Roushan, D. Jaksch, and D. G. Angelakis, *Phys. Rev. Lett.* **117**, 213603 (2016).
 [12] B. Seaman, M. Krämer, D. Anderson, and M. Holland, *Phys. Rev. A* **75**, 023615 (2007).
 [13] L. Amico, A. Osterloh, and F. Cataliotti, *Phys. Rev. Lett.* **95**, 063201 (2005).
 [14] L. Amico, G. Birkel, M. Boshier, and L.-C. Kwek, *New J. Phys.* **19**, 020201 (2017).
 [15] J.-P. Brantut, J. Meineke, D. Stadler, S. Krinner, and T. Esslinger, *Science* **337**, 1069 (2012).
 [16] S. Krinner, D. Stadler, D. Husmann, J.-P. Brantut, and T. Esslinger, *Nature* **517**, 64 (2015).
 [17] D. Husmann, S. Uchino, S. Krinner, M. Lebrat, T. Giamarchi, T. Esslinger, and J.-P. Brantut, *Science* **350**, 1498 (2015).
 [18] S. Krinner, T. Esslinger, and J.-P. Brantut, *J. Phys. Condens. Matter* **29**, 343003 (2017).
 [19] R. Dumke, Z. Lu, J. Close, N. Robins, A. Weis, M. Mukherjee, G. Birkel, C. Hufnagel, L. Amico, M. G. Boshier, *et al.*, *J. Opt.* **18**, 093001 (2016).
 [20] K. C. Wright, R. B. Blakestad, C. J. Lobb, W. D. Phillips, and G. K. Campbell, *Phys. Rev. Lett.* **110**, 025302 (2013).
 [21] A. Ramanathan, K. C. Wright, S. R. Muniz, M. Zelan, W. T. Hill, C. J. Lobb, K. Helmerson, W. D. Phillips, and G. K. Campbell, *Phys. Rev. Lett.* **106**, 130401 (2011).
 [22] C. Ryu, P. W. Blackburn, A. A. Blinova, and M. G. Boshier, *Phys. Rev. Lett.* **111**, 205301 (2013).
 [23] S. Eckel, J. G. Lee, F. Jendrzejewski, N. Murray, C. W. Clark, C. J. Lobb, W. D. Phillips, M. Edwards, and G. K. Campbell, *Nature* **506**, 200 (2014).
 [24] L. Amico, D. Aghamalyan, F. Auksztol, H. Crepaz, R. Dumke, and L. C. Kwek, *Sci. Rep.* **4** (2014).
 [25] D. Aghamalyan, M. Cominotti, M. Rizzi, D. Rossini, F. Hekking, A. Minguzzi, L. C. Kwek, and L. Amico, *New J. Phys.* **17**, 045023 (2015).
 [26] D. Aghamalyan, N. Nguyen, F. Auksztol, K. Gan, M. M. Valado, P. Condylis, L. Kwek, R. Dumke, and L. Amico, *New J. Phys.* **18**, 075013 (2016).
 [27] D. Aghamalyan, L. Amico, and L. C. Kwek, *Phys. Rev. A* **88**, 063627 (2013).
 [28] A. C. Mathey and L. Mathey, *New J. Phys.* **18**, 055016 (2016).
 [29] T. Haug, J. Tan, M. Theng, R. Dumke, L.-C. Kwek, and L. Amico, *Phys. Rev. A* **97**, 013633 (2018).
 [30] T. Haug, L. Amico, R. Dumke, and L.-C. Kwek, *Quantum Sci. Technol.* **3**, 035006 (2018).
 [31] J. Dalibard, F. Gerbier, G. Juzeliūnas, and P. Öhberg, *Rev. Mod. Phys.* **83**, 1523 (2011).
 [32] P. Zupancic, P. M. Preiss, R. Ma, A. Lukin, M. E. Tai, M. Rispoli, R. Islam, and M. Greiner, *Opt. Express* **24**, 13881 (2016).
 [33] T. Haase, D. White, D. Brown, I. Herrera, and M. Hoogerland, *Rev. Sci. Instrum.* **88**, 113102 (2017).
 [34] G. Gauthier, I. Lenton, N. M. Parry, M. Baker, M. Davis, H. Rubinsztein-Dunlop, and T. Neely, *Optica* **3**, 1136 (2016).
 [35] L. Jiang, T. Kitagawa, J. Alicea, A. Akhmerov, D. Pekker, G. Refael, J. I. Cirac, E. Demler, M. D. Lukin, and P. Zoller, *Phys. Rev. Lett.* **106**, 220402 (2011).
 [36] C. Muldoon, L. Brandt, J. Dong, D. Stuart, E. Brainis, M. Himsforth, and A. Kuhn, *New J. Phys.* **14**, 073051 (2012).
 [37] K. Henderson, C. Ryu, C. MacCormick, and M. G. Boshier, *New J. Phys.* **11**, 043030 (2009).
 [38] T. Haug, H. Heimonen, R. Dumke, L.-C. Kwek, and L. Amico, *arXiv:1706.05180* (2017).
 [39] T. Haug, R. Dumke, L.-C. Kwek, and L. Amico, *arXiv:1807.03616* (2018).
 [40] R. Citro and F. Romeo, *Phys. Rev. B* **73**, 233304 (2006).
 [41] P. Marra, R. Citro, and C. Ortix, *Phys. Rev. B* **91**, 125411 (2015).
 [42] Q. Niu and D. Thouless, *J. Phys. A* **17**, 2453 (1984).
 [43] Y. He, K. Wright, S. Kouachi, and C.-C. Chien, *Physical Review A* **97**, 023618 (2018).
 [44] L. Amico, A. Osterloh, and U. Eckern, *Phys. Rev. B* **58**, R1703 (1998).
 [45] E. Compagno, L. Banchi, C. Gross, and S. Bose, *Phys. Rev. A* **95**, 012307 (2017).
 [46] E. Torrontegui, S. Ibáñez, S. Martínez-Garaot, M. Modugno, A. del Campo, D. Guéry-Odelin, A. Ruschhaupt, X. Chen, and J. G. Muga, in *Adv. At. Mol. Opt. Phys.*, Vol. 62 (Elsevier, 2013) pp. 117–169.
 [47] P. Roushan, C. Neill, A. Megrant, Y. Chen, R. Babbush, R. Barends, B. Campbell, Z. Chen, B. Chiaro, A. Dunsworth, *et al.*, *Nat. Phys.* **13**, 146 (2017).

Scaling of the energy gap

The energy gap between the pumped many-body energy level and the next level determines the rate of non-adiabatic Landau-Zener transitions. To avoid these transitions the driving must be $\Omega \ll \Delta E$. In Fig.6, we plot the energy gap to

the next level at the crossing point for convex and concave band curvature. In the following, we derive the many-body energy gap for for concave crossings. We consider a reduce model, consisting of two neighboring sites only. Other sites can be neglected due to the large potential difference. We indicate the many-body states of this two-site model as $|N_1, N_2\rangle$, where N_1 (N_2) is the number of particles at the first (second) site. For concave, the many-body states are resonantly coupled. As a result, for e.g. $N = 3$, the following resonant transitions occur one after the other due to the adiabatic driving: $|30\rangle \rightarrow |21\rangle \rightarrow |12\rangle \rightarrow |03\rangle$. For $|U| \gg J$, the minimal energy gap is given by $\Delta E = 2\sqrt{N}J$. It can be derived by degenerate perturbation theory (for $P_0 \gg U \gg J$). At a specific point in time, two many-body states will have the same local energy (potential plus interaction energy). All other many-body states are far off-resonant. The two resonant states are weakly coupled by the hopping strength J . Giving an example for states $|N, 0\rangle$ and $|N-1, 1\rangle$ and $U > 0$: The local energy of many-body state $|N, 0\rangle$ is $E_1 = -NP_0 \cos(\Omega t) + \frac{U}{2}N(N-1)$, and of $|N-1, 1\rangle$ $E_2 = -(N-1)P_0 \cos(\Omega t) - P_0 \cos(2\pi/3 + \Omega t) + \frac{U}{2}(N-1)(N-2)$. For a time t^* , both levels are degenerate $E_1(t^*) = E_2(t^*)$ with all other many-body states far off-resonant. We can treat them as a two level system within degenerate perturbation theory. The two states are now weakly coupled via the nearest-neighbor hopping $\mathcal{H}_J = J\hat{a}_1^\dagger \hat{a}_2 + \text{H.C.}$. The coupling matrix element is $\langle N, 0 | \mathcal{H}_J | N-1, 1 \rangle = \sqrt{N}J$. The resulting energy splitting is $\Delta E = E_2 - E_1 = 2\sqrt{N}J$. This is the minimal gap for all resonant transitions.

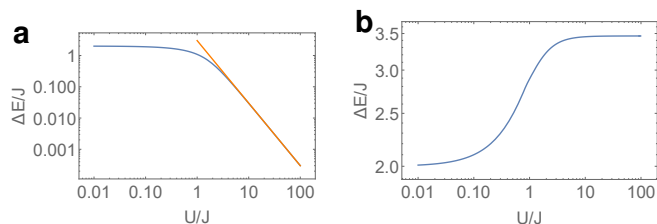


FIG. 6. Scaling of the energy gap ΔE at the transition point from one site to the next as shown in Fig.2b. Energy gap in blue, fit in orange. **a)** Convex, off-resonant coupling ($U > 0$, convex crossing as in band +1). For small U , gap scales as $\Delta E \propto J^N/U^{N-1}$, indicated in orange (here $N = 3$). To avoid non-adiabatic Landau-Zener transitions, the driving speed must be $\Omega \ll \Delta E$. Gap is largest for $U < J$. **b)** Scaling of the energy gap ΔE for resonant transitions ($U > 0$, concave crossing as in band -1). Energy gap $\Delta E = 2\sqrt{N}J$ is independent of U for $|U| \gg J$.

Creating NOON states

Here, we go in further detail how to create NOON states. The relevant part of our setup is the lead-ring junction, where one input site is connected to two output sites via tunneling. We remove all other sites of the setup. We initialize the particles at the input site, and evolve the system. Depending on ϕ_0 of the potential, the state after the pumping is either a NOON

state or a product state. We can see this from the nature of the transitions: If the transition is resonant (concave case, $\phi_0 = \pi$), the tunneling from one site to the next occurs via occupying the intermediate many-body states one after the other, meaning one after the other particle tunnels over when the state becomes resonant due to the driving. e.g. for $N = 2$ and same notation as in Fig.2c, $|200\rangle \rightarrow |110\rangle + |101\rangle \rightarrow |011\rangle$. The end result is a product state.

In the case of off-resonant transition (convex case, $\phi_0 = 0$), the tunneling can only occur when the final states have the same energy, e.g. $|200\rangle$ and $|020\rangle + |002\rangle$. This happens off-resonantly via weakly occupied intermediate states. In this case, the particles tunnel together as a whole.

Interaction dependence

In this section we study the transmission into the drain for varying interaction at different values of flux and particle number. For band +1 and -1, see Fig.7. For the central band 0, see Fig.8.

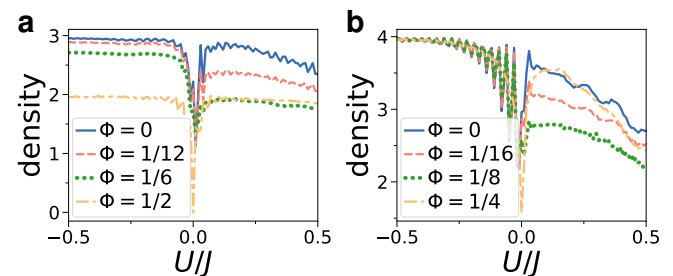


FIG. 7. Density pumped through the ring into the drain plotted against interaction strength for band +1 (For dynamics of band -1, invert interaction $U \rightarrow -U$). **a)** 3 particles: for $U < 0$ AB effect changes particle number in drain between 3 and 2, with minimum for $\Phi = 1/2$. For $U > 0$ same change in density, however with minimum at $\Phi = 1/6$. **b)** 4 particles: for $U < 0$ independent of flux, while for $U > 0$ minimum at $\Phi = 1/8$. Close to $U \approx 0$, minimal density for $\Phi = 1/2$. The number of particle pumped into the drain decreases for larger U due to Landau-Zener transitions as the gap decreases, while for negative interactions it does not change with large negative interactions. The strong oscillations at small U result from non-adiabatic transitions when $U \approx \Omega$. Drain density taken at $tJ = 1260$ with $L_R = 8$, $\Omega = 0.01J$ and $P_0 = 60J$.

Two species pumping

One can also consider a different setup: The same Hamiltonian as introduced in the main text with now two species of atoms (denoted as \uparrow, \downarrow). There is only one particle of each species. The two species interact with

$$\mathcal{H}_{\text{int}} = \sum_j U \hat{n}_j^\uparrow \hat{n}_j^\downarrow \quad (4)$$

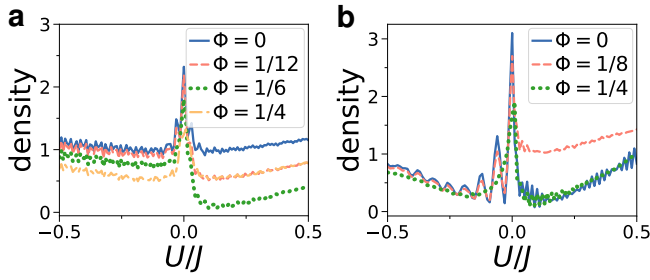


FIG. 8. Density pumped through the ring into the drain for central band with Chern number $C = 2$. Here, band 0^+ with initial condition $\phi_0 = \pi/2$ was chosen. (For dynamics of band 0^- , invert interaction $U \rightarrow -U$) **a)** Dependence on interaction U for different values of flux Φ for $N = 3$ particles and **b)** for $N = 4$ particles. Drain density taken at $tJ = 630$ with $L_R = 8$, $\Omega = -0.01J$ and $P_0 = 60J$.

Driving this setup for the lower band -1 generates Bell states in the ring $|\Psi_+\rangle \propto |\uparrow\downarrow\rangle + |\downarrow\uparrow\rangle$ (indicating states as $|\uparrow\downarrow\rangle$). The pumping is flux independent. For the upper band +1 we

observe NOON states.

In Fig.9, we present the transmitted density for pumping of 2 species of atoms.

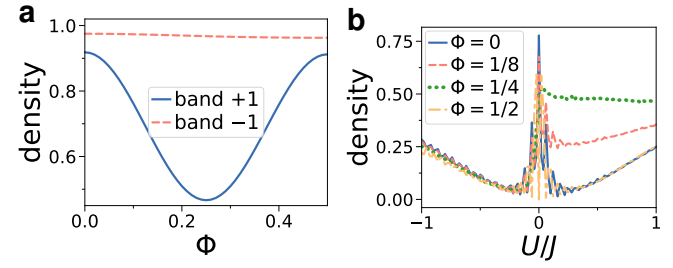


FIG. 9. Density pumped through the ring into the drain for 2 species of atoms, with one atom for each species. **a)** $L = 8$, $U = 0.5$ **b)** interaction dependence for central band with ring length $L_R = 8$ and initial condition 0^+ .